Nano-ordered topographical effects on dissociation of carboxylic acid terminated self-assembled monolayers adsorbed onto a gold surface

Masato Tominaga,* Shouko Maetsu, Atsushi Kubo and Isao Taniguchi*

Corresponding author:

Graduate School of Science and Technology,

Kumamoto University

2-39-1 Kurokami, Kumamoto 860-8555 (Japan)
Fax: (+81)963423656
E-mail: masato@gpo.kumamoto-u.ac.jp

Abstract

A nano-ordered topographical surface (0.8~1.6 nm) was prepared by the modification of gold nanoparticles on an evaporated Au film. Nano-ordered topographical effects for the protonation-deprotonation behaviors of 10-carboxy-1-decanethiol (CDT) monolayers adsorbed onto a gold surface were then demonstrated by the use of $[Ru(NH_3)_6]^{3+}$ as a redox probe. On the assumption that current of $[Ru(NH_3)_6]^{3+}$ on the CDT modified electrode is composed to two independent parts of the protonated and deprotonated CDT, the titration curve for the redox peak current values obtained from cyclic voltammograms of $[Ru(NH_3)_6]^{3+}$ as a function of pH was analyzed by a statistical mechanical model for water-solid interfaces (1-pKa model). The results obtained strongly suggest that the electrostatic repulsion of the carboxylic acid terminated self-assembled monolayer adsorbed onto a gold surface with nano-ordered topography was much smaller than that adsorbed on an atomically flat gold surface, which was also supported by reflection FTIR measurements.

Keywords: gold surface, self-assembled monolayer, electrode, carboxylic acid, gold nanoparticles

1. Introduction

The formation and structure of self-assembled monolayers (SAMs) based on thiolate-metal bonding have been well-characterized as a model system for understanding organic monolayer interfaces [1-12]. SAMs containing carboxyl or amino groups have been used to immobilize proteins and other functional compounds [13] and quantitative measurements of the acid/base properties of these SAMs have been extensively investigated [14-18]. In previous studies, usually, an atomically flat surface has been typically used as the substrate for the modification of SAMs. Functional SAM groups modified on nano-ordered topographical surfaces would show different behaviors as compared to those modified on atomically flat surfaces, since a relatively strong interaction of the terminal functional groups of neighboring SAMs adsorbed onto an atomically flat surface would be expected. Recently, the effects of gold substrate topographies on the formation and structure of SAMs, and ultimately, the adsorption and electron transfer reactions of heme proteins such as cytochrome c have been investigated [19].

Investigations into nano-ordered topographical surfaces are essential for understanding nano topographical effects. In this study, a nano-ordered topographical surface, as shown in Fig. 1, was prepared by the modification of gold nanoparticles (Au-NPs) on an evaporated Au film (Au/mica). Furthermore, the protonation-deprotonation behaviors of carboxylic acid terminated self-assembled monolayers adsorbed onto these nano-ordered topographical gold surfaces as compared to smooth surfaces were investigated by their electrochemical reactions with redox species and reflection FTIR measurements. The results obtained suggest that the protonation-deprotonation behavior of the self-assembled monolayer functional group is strongly influenced by its adsorption surface topography.

2. Experimental Section

The substrate of a gold thin film on mica (Au/mica) was prepared by the vapor deposition of 100 nm of gold (99.999% purity) onto freshly cleaved mica sheets (Nilaco Co., Japan) at a reduced pressure, $< 0.1 \times 10^{-6}$ Torr. The temperature of the mica sheet was maintained at 350 ˚C during the vapor deposition. The prepared Au/mica surface was atomically flat as shown in Fig. 2. Cyclic voltammograms of the gold thin film surface on mica in a 0.01 mol dm^{-3} $HClO_4$ solution indicated that the gold surface was enriched with Au(111) facets [11]. Gold nanoparticles of ~2 nm cores capped with decanethiolate monolayer shells (DT-Au nanoparticles) were synthesized by Schiffrin's two-phase synthesis protocol [20,21]. Briefly, 0.75 mmol hydrogen tetrachloroaurate (III) trihydrate (Aldrich, $HAuCl_4\,3H_2O$, 99.9+ %) was dissolved in 25 mL of a purified water solution. To transform $AuCl_4^-$ from the aqueous phase to the toluene phase, a $HAuCl_4$ aqueous solution was added to 80 mL toluene containing tetraoctylammonium bromide (Lancaster, TOAB, 98 %, 3.0 mmol) as a phase transfer reagent. DT (Aldrich, DT, 96 %) was added to the toluene phase at a 2:1 DT/Au ratio to act as a capping agent. An aqueous solution (25 mL) of 20 mmol $NaBH_4$ (Aldrich, 99.995 %) was added drop wise to this solution as a reducing agent. The newly-synthesized DT-Au nanoparticles were then purified by multiple wash steps using ethanol. Next, the nanoparticles were dried and dissolved in hexane. The average core size of the DT-Au nanoparticles was determined to be 2.3 (± 1.0) nm by transmission electron microscopy (TEM).

The electrochemical measurements were carried out in a three-electrode cell. Cyclic voltammetric measurements were performed in solutions of various pH values using an electrochemical analyzer (Bioanalytical Systems, BAS 100B/W). An Ag/AgCl (saturated KCl) electrode and a platinum electrode were used as the reference and counter electrodes, respectively. All potentials are reported with respect to the Ag/AgCl (saturated KCl) electrode. Prior to the cyclic voltammetric measurements, the buffer solution was de-aerated with high

purity nitrogen, and a positive pressure of nitrogen was kept over the solution during all electrochemical experiments.

The FTIR reflection spectra were obtained using a Bio-Rad FTS-6000 spectrometer, which was purged with dry-nitrogen gas. The spectrometer was equipped with a liquid nitrogen-cooled HgCdTe detector. The incident angle was 75˚ with respect to the surface normal. The samples were immersed into solutions of various pH values (5 mmol dm^{-3} HCl and NaOH), followed by evaporation of the water.

X-ray photoelectron spectroscopy (XPS) measurements were then performed using a Thermo VG Scientific, Sigma Probe HA6000II. This instrument uses a focused monochromatic Al Kα X-ray (1486.68 eV) source for excitation, a spherical section analyzer, and a 6-element multichannel detection system.

3. Results and discussion

3.1. Preparation of nano-ordered topographical gold surface

The nano-ordered topographical gold surface was prepared as follows, as shown in Fig. 2: The Au/mica was annealed by a hydrogen flame, followed by immersion into an ethanol solution of 1 mmol dm^{-3} 1,9-nonane-dithiol (NDT, Aldrich, 95 %) for 24 hours to create a monolayer film of NDT on the Au/mica. Next, the NDT-modified Au/mica was immersed into DT-Au nanoparticles (in hexane) for 24 hours. To inhibit oxidation of the surfer moiety of NDT, this surface modification process was carried out under UV-protected conditions [22]. After this process, the monolayer modification of the Au nanoparticles onto a Au/mica was performed as shown in Fig. 2. To remove the monolayer organic encapsulate from the nanoparticles and NDT, the modified substrate was heated from room temperature to 250 ˚C for 30 min under an air atmosphere using a muffle furnace. After the heat-treatment, atomic force microscopy (AFM) measurements indicated that the prepared electrode surface (NPs-

Au/mica) had a nano-ordered topography. Aside from the full coverage modification of Au-NPs onto the Au/mica, to estimate the unevenness of the surface, a low Au-NPs coverage surface was prepared, followed by the heat-treatment. As shown in Fig. 3, the unevenness of the surface was evaluated to be *ca*. 0.8 - 1.6 nm based on the AFM measurements. From the obtained results, we believed that the nano-ordered topographical surface had an unevenness of 0.8 – 1.6 nm. The elimination of organic species (DT and NDT) from the substrate by heat-treatment was confirmed by XPS and IR measurements. Before the heat-treatment, bands corresponding to asymmetric and symmetric methylene stretching, $\nu_{a,s}(CH_2)$ (2921 and 2852 cm^{-1}, respectively), and bands corresponding to asymmetric and symmetric methyl stretching, $\nu_{a,s}(CH_3)$ (2956 and 2872 cm^{-1}, respectively) were observed by the FTIR reflection spectra. Bands corresponding to diagnostic C-H bending, wagging and C-C stretching modes were also observed in the low-frequency region around 1150 – 1400 cm^{-1}. After the heat-treatment, C-H alkyl chains representing absorption bands in both the high-frequency region of 2800 – 3000 cm^{-1} and the low-frequency region of 1150 – 1400 cm^{-1} disappeared completely. Peaks corresponding to S(2p) bands (162.5 and 163.5 eV) were also undetectable by XPS measurement after the heat-treatment.

3.2. Characterization of CDT monolayers modified on nano-ordered topographical gold surface

Pre-treated NPs-Au/mica and Au-mica electrode surfaces were modified with SAMs of 10-carboxy-1-decanethiol (CDT, 97 % <, Dojin Chem. Co., Japan) by immersion into 2 mmol dm^{-3} CDT (ethanol) for 20 min, according to the methods described in previous papers [23]. The surface coverage of CDT on the Au/mica electrode was estimated to be 8.2 (± 0.3) x 10^{-10} mol cm^{-2} by voltammograms recorded in a 0.1 mol dm^{-3} KOH solution (Fig. 4). The results indicated that full coverage CDT monolayers had formed on the Au/mica surface. The

roughness factors of this surface were evaluated to be 1.1 based on the reported full coverage monolayers value of 7.6 x 10^{-10} mol cm^{-2} [12]. Also, the surface coverage of CDT on NPs-Au/mica was estimated to be 8.2 (± 0.3) x 10^{-10} mol cm^{-2}. No clear difference in the coverage of adsorbed CDT between the NPs-Au/mica and Au/mica electrodes was recognized in the measurement error. This is surprising result. In general, everybody expects that the surface coverage value of CDT on NPs-Au/mica surface is lager than that on Au/mica surface, because the NPs-Au/mica surface area is much larger than the Au/mica surface area.

We thought the expected surface model as shown in Fig. 5 to understand the surface coverage of CDT on NPs-Au/mica and Au/mica surfaces. First, the surface area of NPs-Au/mica is calculated as shown in Fig. 5, which is given eq. 4 .

$$S_1 = \frac{(2+a)^2}{2}\sqrt{3}r^2 \tag{1}$$

$$S_2 = \frac{4\pi r^2}{2} \times \frac{2L^2}{(2+a)^2\sqrt{3}r^2} = \frac{4\pi L^2}{(2+a)^2\sqrt{3}} \tag{2}$$

$$S_3 = L^2 - \pi r^2 \times \frac{2L^2}{(2+a)^2\sqrt{3}r^2} = \left(1 - \frac{2\pi}{(2+a)^2\sqrt{3}}\right) L^2 \tag{3}$$

$$S_{NPs\text{-}Au} = S_2 + S_3 = \frac{4\pi L^2}{(2+a)^2\sqrt{3}} + \left(1 - \frac{2\pi}{(2+a)^2\sqrt{3}}\right) L^2 = \left(\frac{2\pi}{(2+a)^2\sqrt{3}} + 1\right) L^2 \tag{4}$$

where S_1 is diamond unit area as shown in Fig. 5, S_2 is the total surface area of semisphere in the LxL surface area, S_3 is the total area of the LxL area subtracted semisphere occupied area, and $S_{NPs\text{-}Au}$ is the total surface area of the model.

Then, the surface area of NPs-Au/mica is $[2\pi /((a + 2)^2 \sqrt{3}) + 1]$ times larger than that of Au/mica: For example, the surface area ratios of (NPs-Au/mica)/(Au/mica) are 1.9 for a = 0 (hexagonal packed), 1.4 for a = 1 and 1.2 for a = 2. From the results of calculated surface

area, it is expected that the surface coverage of CDT on the NPs-Au/mica electrode is larger than that on Au/mica. Next, the expected adsorption models of CDT on NPs-Au/mica and Au/mica surface are prepared as shown in Fig. 6. The molecular size and its occupied surface area are taken in account. Fig. 6A shows the model for CDT on Au/mica surface. About 30 molecules exist on the diamond unit surface area (6.3 nm^2). Fig. 6B, C and D show the models for CDT on NPs-Au/mica surface, when the nanoparticles exist on the surface with inter-hemispherical nanoparticles distance of 0, 1 and 2 nm, respectively. The molecular number of CDT on NPs-Au/mica surface is evaluated to be ca. 30 molecules on the diamond unit surface area, even if the hemispherical nanoparticles exist like a hexagonal packed. No dependence in the molecular number on those surfaces is identified. It is noteworthy that, when surface coverage of molecules on surface with nano-ordered topography is evaluated, it must be take in account of nano-ordered topographical size, molecular size, and its molecular steric hindrance. Taking in account the reason described above, it can be understood that no clear difference in the coverage of adsorbed CDT between the NPs-Au/mica and Au/mica electrodes was observed.

On the reductive desorption curves of CDT, the different behaviors were recognized. As shown in Fig. 4, the peak shape of the reduction curve for CDT on the NPs-Au/mica electrode was broader than that on the Au/mica electrode. The values for the peak width at half maximum and the reduction peak potential at the NPs-Au/mica and Au/mica electrodes were 34 and 24 mV, and -0.93 and -0.96 V, respectively. It is well-known that the reductive desorption of carboxylic acid terminated SAMs yields a very narrow voltammetric peak in 0.5 mmol dm^{-3} KOH solution, although all of the carboxyl groups should be dissociated and are negatively charged. This behavior has been understood to be due to the strong attractive interactions, which are derived from the alleviation of electrostatic repulsion and the endowment of attractive interaction by the counter ion binding to the surface carboxyl groups

under a relatively higher ionic strength condition (0.1 mol dm^{-3} KOH) [18]. These results, together with the fact that the both surface coverage of CDT adsorbed onto the NPs-Au/mica and Au/mica electrodes were the same suggested that the carboxyl group of the CDT monolayer was more ordered on the Au/mica surface than on the NPs-Au/mica surface.

3.3. Titration curves of dissociation of carboxylic acid obtained from cyclic voltammograms of $[Ru(NH_3)_6]^{3+}$ and its simulated analysis

Fig. 7 shows cyclic voltammograms of $[Ru(NH_3)_6]^{3+}$ at the CDT-modified NPs-Au/mica (CDT-NPs-Au/mica) and CDT-modified Au/mica (CDT-Au/mica) electrodes at various pH values. At the pH < 4 region, no redox response for $[Ru(NH_3)_6]^{3+}$ was observed at both CDT-NPs- and CDT- Au/mica electrodes. On the other hand, at the pH > 4 region, the redox current increased with increasing pH. The anodic peak current (I_{pa}) in the voltammogram was plotted vs. the pH as shown in Fig. 8. The I_{pa} vs. pH profile at CDT-Au-NPs-Au/mica electrode changed drastically at pH 4, and the I_{pa} remained almost constant at pH values higher than 7.5. The aforementioned behavior is reasonable because the electrode reactions of positively charged $[Ru(NH_3)_6]^{3+}$ are promoted at surfaces with a $–COO^-$ rather than at surfaces with –COOH, as in CDT. In the case of the CDT-Au/mica electrode, the I_{pa} increased at pH 4. However, at pH values higher than 4, a gradual increase in the I_{pa} with increasing pH values was observed. The previous behavior would be indicative of a deprotonation of the –COOH as the CDT adsorbed onto the Au/mica occurred more slowly than that adsorbed onto the NPs-Au/mica.

The surface pKa of CDT would be determined from the current parameter of cyclic voltammograms of $[Ru(NH_3)_6]^{3+}$ at the CDT-modified NPs-Au/mica (CDT-NPs-Au/mica) and CDT-modified Au/mica (CDT-Au/mica) electrodes at various pH values. As described

above, the redox peak current (I_{pa}) of $[Ru(NH_3)_6]^{3+}$ was dependent on the pH of bulk solutions. Thus, the I_{pa} would be conveniently used to investigate the dissociation of carboxylic acid of CDT. According to the definition of pKa in a bulk solution, the surface pKa can be defined from ionization equilibrium of the carboxylic acid of CDT:

$$[AH] = [A^-] + [H^+] \qquad (5)$$

$$Ka = [A^-][H^+]/[AH]$$

where [AH] and $[A^-]$ are the surface concentrations of deprotonated and protonated carboxylic acid of CDT, respectively. Assuming the peak current of the redox specie on the CDT modified electrode is composed to two independent parts, one through the deprotonated CDT, $[A^-]$, and the other through the protonated CDT, [AH], then Ipa can be described as follows:

$$I_{pa} = I_{A^-}[A^-] + I_{AH}[AH] \qquad (6)$$

where I_{A^-} and I_{AH} are currents of the redox specie on the CDT fabricated by $[A^-]$ and [RH] structures, respectively. By using $[A^-] + [AH] = 1$ and $\theta = [A^-] / ([A^-] + [AH])$ and equation 6, the following equation ca be obtained:

$$I_{pa} = I_{A^-}\theta + I_{AH}(1-\theta) \qquad (7)$$

$$0 \le \theta \le 1$$

Where I_{A^-} and I_{AH} can be determined by the average values at low pH (< 4) and high pH (> 9). The anodic peak current (I_{pa}) in the voltammogram was plotted vs. θ as shown in Fig. 8.

The surface p*Ka* for carboxylic acid terminated self-assembled monolayers on Au surfaces has been reported to be *ca.* 5-9 [14-17], and the reported values lack agreement

among various researchers. However, these reported values are *ca.* 1-5 pH units more alkaline than those of alkanoic acids in a homogeneous aqueous solution. Several factors can cause an increase in the p*Ka*: repulsive interactions between deprotonated groups, hydrogen bonding and a lower dielectric constant in the inner part of the double layer [14-17]. The effect of electrostatic repulsion on the protonation-deprotonation characteristics is well known in weak polyelectrolytes. On the assumption that the peak current of $[Ru(NH_3)_6]^{3+}$ on the CDT modified electrode is composed to two independent parts of the protonated and deprotonated CDT, we tried to analyze the results of the I_{pa} (or θ) vs. pH profiles by 1-pKa model [16,17]. The titration curves are as follows:

$$\text{pH} - \text{p}Ka = \log\frac{\theta}{1-\theta} + \frac{\beta\bar{E}\,\theta}{2.303} \qquad (8)$$

where p*Ka* is the intrinsic p*Ka* value in the absence of intermolecular interaction, θ is the degree of dissociation, $\beta = 1/RT$, and $\bar{E}$ is the potential of mean force arising from the electrostatic interaction of a charged molecule to its surroundings. The best fit to the experimental curves of I_{pa} vs. pH for both CDT-NPs- and CDT- Au/mica electrodes was obtained when p*Ka* = 6.0 was used, and $\beta\bar{E}$ = 1 and 4 were used for the CDT-NPs- and CDT-Au/mica electrodes, respectively, as shown in Fig. 8. The $\beta\bar{E}$ = 4 value of CDT adsorbed onto Au/mica was in agreement with the value ($\beta\bar{E}$ = 3) estimated by the double-layer capacitance titration method using an Au/mica electrode [17]. The increase in the $\beta\bar{E}$ value means an increase in the order of the electrostatic repulsion. The results obtained strongly suggest that the electrostatic repulsion of CDT adsorbed onto the NPs- Au/mica electrode was much smaller than that of CDT adsorbed onto the Au/mica electrode. For an in-depth understanding of the obtained p*Ka* value, one should take into account microscopic

environmental conditions, for example the electrolyte concentration, electrode potential effect and double-layer interactions [14-17].

3.4. FTIR studies on dissociation behaviors of carboxylic acid

Nano-ordered topographical effects for the dissociation behaviors of carboxylic acid for CDT were also investigated by reflection FTIR measurements [24]. Fig. 9 shows the reflection FTIR spectra for CDT adsorbed onto NPs-Au/mica and Au/mica surfaces. In the pH region < 3, peaks corresponding to the C=O stretching of -COOH (*ca*. 1717 and 1738 cm^{-1}) were observed [3,15,24,25]. As the pH increased, the C=O stretching peaks gradually decreased. On the other hand, peaks corresponding to the asymmetric and symmetric stretching of $-COO^-$ (ca. 1440 and 1581-1600 cm^{-1}, respectively) increased [3,15,24,25]. In the pH region 3~10, the detection of both –COOH and $-COO^-$ species was indicative of a partial protonation-deprotonation process. Eventually, in the pH region > 10, the peaks representing -COOH completely disappeared, and peaks representing $-COO^-$ only were present. Symmetric stretching peaks from $-COO^-$ observed on CDT-Au/mica were not identified on the CDT-NPs-Au/mica surface. The previous phenomenon could be due to the quite broad band for hydrogen bonding and/or the parallel orientation of the carbonyl group with respect to the plane of the gold surface [3]. Fig. 10 shows the ratio of the peak area representing COO^- against that representing COOH, as a function of pH. This plot clearly indicates that a deprotonation of the CDT modified onto NPs-Au/mica was favored with respect to CDT modified onto Au/mica. The deprotonation behavior was in agreement with that deteremined by cyclic voltammograms using $[Ru(NH_3)_6]^{3+}$ as a redox probe. This fact would be indicate that the assumption is reasonable that the peak current of $[Ru(NH_3)_6]^{3+}$ on the CDT modified electrode is composed to two independent parts of the protonated and deprotonated CDT.

4. Conclusions

We prepared the electrode surface with a nano-ordered topography (0.8~1.6 nm). Nano-ordered topographical effects for the protonation-deprotonation behaviors of carboxylic acid terminated self-assembled monolayers adsorbed on a gold surface was demonstrated by the use of $[Ru(NH_3)_6]^{3+}$ as a redox probe. On the assumption that current of $[Ru(NH_3)_6]^{3+}$ on the CDT modified electrode is composed to two independent parts of the protonated and deprotonated CDT, the titration curve for the anodic peak current values obtained from the cyclic voltammograms of $[Ru(NH_3)_6]^{3+}$ as a function of pH was analyzed by 1-pKa model. The obtained results strongly suggest that the electrostatic repulsion of a carboxylic acid terminated self-assembled monolayer adsorbed onto a gold surface with nano-ordered topography was much smaller than that adsorbed onto an atomically flat gold surface, which was also supported by reflection FTIR measurements. The results obtained would be suggest that the protonation-deprotonation behavior of the self-assembled monolayer functional group is strongly influenced by its adsorption surface topography.

Acknowledgements

This work was supported in part by a Grand-in-Aid for Scientific Research (M. T.) from the Ministry of Education, Culture, Science, Sports and Technology of Japan.

References

[1] W. C. Bigelow, D. L. Pickett, W. A. Zisman, J. Colloid Interface Sci. 1 (1946) 513.

[2] R. G. Nuzzo, D. L. Allara, J. Am. Chem. Soc. 105 (1983) 105, 4481; D. L. Allara, R. G. Nuzzo, Langmuir 1 (1985) 45; D. L. Allara, R. G. Nuzzo, Langmuir 1 (1985) 52; L. H. Dubois, B. R. Zegarski, R. G. Nuzzo, J. Am. Chem. Soc. 112 (1990) 570; L. H. Dubois, B. R. Zegarski, R. G. Nuzzo, J. Chem. Phys. 98 (1993) 678.

[3] N. E. Schlotter, M. D. Poter, T. B. Bright, D. L. Allara, Chem. Phys. Lett. 132 (1986) 93; E. B. Troughton, C. D. Bain, G. M. Whitesides, R. G. Nuzzo, D. L. Allara, M. D. Porter, Langmuir 4 (1988) 365.

[4] M. D. Porter, T. B. Brigth, D. L. Allara, C. E. D. Chidsey, J. Am. Chem. Soc. 109 (1987) 3559; C. E. D. Chidsey, Science 251 (1991) 919; C. E. D. Chidsey, C. R. Bertozzi, T. M. Putvinski, A. M. Mujsce, J. Am. Chem. Soc. 112 (1990) 4301.

[5] C. D. Bain, G. M. Whiteside, Science 240 (1988) 62; S. R. Waasserman, Y.-T. Tao, G. M. Whiteside, Langmuir 5 (1989) 1074; G. M. Whitesides, P. E. Laibinis, Langmuir 6 (1990) 87; T. Randall Lee, R. I. Carey, H. A. Biebuyck, G. M. Whitesides, Langmuir 10 (1994) 741.

[6] A. Ulman (Ed.), Characterization of Organic Thin Films, Butterworth-Heineman, Stoneham, MA, 1994; A. Ulman (Ed.), An Introduction to Ultrathin Organic Films from Langmuir-Blodgett to Self-Assembly, Academic, San Diego, CA, 1991; H. O. Finklea (Ed.), Electrochemistry of organized monolayers of thiols and related molecules on electrodes, Electroanalytical Chemistry: A Series of Advances, Electroanalytical Chemistry 19, Marcel Dekker, NY, 1996.

[7] Y.-T. Tao, J. Am. Chem. Soc. 115 (1993) 4350; Y.-T. Tao, M.-T. Lee, S.-C. Chang, J. Am. Chem. Soc. 115 (1993) 9547.

[8] Y.-T. Kim, R. L. McCarley, A. J. Bard, Langmuir 9 (1993) 1941; McCarley, Y.-T. Kim, A. J. Bard, J. Phys. Chem. 97 (1993) 211.

[9] A. Ulman, Chem. Rev. 96 (1996) 1533.

[10] C. A. Widrig, C. A. Alves, M. D. Porter, J. Am. Chem. Soc. 113 (1991) 2805; C. A. Alves, E. L. Smith, M. D. Porter, J. Am. Chem. Soc. 114 (1992) 1222; E. L. Smith, M. D. Poter, J. Phys. Chem. 97 (1993) 4421; C. J. Zhong, M. D. Porter, Anal. Chem. 67 (1995) 709A.

[11] K. Uosaki, Y. Shen, T. Kondo, J. Phys. Chem. 99 (1995) 14117.

[12] C. A. Widrig, C. Chung, M. D. Porter, J. Electroanal. Chem. 310 (1991) 335.

[13] M. J. Tarlov, E. F. Bowden, J. Am. Chem. Soc. 113 (1991) 1847; Z. Q. Feng. S. Imabayashi, T. Kakiuchi, K. Niki, J. Chem. Soc., Faraday Trans. 93 (1997) 1367; L. J. Kepley, R. M. Crooks, A. J. Ricco, Anal. Chem. 64 (1992) 3191; C. E. Jordan, B. L. Frey, S. Korngruth, R. M. Corn, Langmuir 10 (1994) 3642; S. Terrettaz, J. Cheng, C. J. Miller, R. D. Guiles, J. Am. Chem. Soc. 118 (1996) 7857; G. B. Sigal, M. Mrksich, G. M. Whitesides, J. Am. Chem. Soc. 120 (1998) 3464; X.-Y. Hu, Y. Xiao, H.-Y. Chen, J. Electroanal. Chem. 466 (1999) 26; M. Tominaga, A. Ohira, A. Kubo, I. Taniguchi, M. Kunitake, Chem. Commun. (2004) 1518.

[14] S. E. Creager, J. Clarke, Langmuir 10 (1994) 3675; K. Aoki, T. Kakiuchi, J. Electroanal. Chem. 478 (1999) 101; J. Zhao, L. Luo, X. Yang, E. Wang, S. Dong, Electroanalysis 11 (1999) 1108; K. Hu, A. J. Bard, Langmuir 13 (1997) 5114; V. Kane, P. Mulvaney, Langmuir 14 (1998) 3303; H. S. White, J. D. Peterson, Q. Cui, K. J. Stevenson, J. Phys. Chem. B 102 (1998) 2930; J. F. Smalley, K. Chalfant, S. W. Feldberg, T. M. Nahir, E. F.

Bowden, J. Phys. Chem. B 103 (1999) 1676; K. Shimazu, T. Teranishi, K. Sugihara, K. Uosaki, Chem. Lett. 27 (1998) 669.

[15] K. Sugihara, K. Shimazu, K. Uosaki, Langmuir 16 (2000) 7101.

[16] M. Borkovec, Langmuir 13 (1997) 2608.

[17] T. Kakiuchi, M. Iida, S. Imabayashi, K. Niki, Langmuir 16 (2000) 5397.

[18] J. Li, K. S. Liang, G. Scoles, A. Ulman, Langmuir 11 (1995) 4418; V. Kane, P. Mulvaney, Langmuir 14 (1998) 3303; S. Imabayashi, M. Iida, D. Hobara, Z. Q. Fengg, K. Niki, T. Kakiuchi, J. Electroanal. Chem. 428 (1997) 33.

[19] M. C. Leopold, J. A. Black, E. F. Bowden, Langmuir 18 (2002) 978; M. C. Leopold, E. F. Bowden, Langmuir 18 (2002) 2239; D. Losic, J. G. Shapter, J. J. Gooding, Langmuir 17 (2001) 3307.

[20] M. Brust, M. Walker, D. Bethell, D. J. Schiffrin, R. Whyman, J. Chem. Soc., Chem. Commun. (1994) 801.

[21] M. J. Hostetler, J. E. Wingate, C. J. Zhong, J. E. Harris, R. W. Vachet, M. R. Clark, J. D. Londono, S. J. Green, J. J. Stokes, G. D. Wignall, G. L. Glish, M. D. Porter, N. D. Evans, R. W. Murray, Langmuir 14 (1998) 17.

[22] P. Kohli, K. K. Taylor, J. J. Harris, G. J. Blanchard, J. Am. Chem. Soc. 120 (1998) 11962.

[23] M. Tominaga, A. Ohira, A. Kubo, I. Taniguchi, M. Kunitake, Chem. Commun. (2004) 1518; M. Tominaga, A. Ohira, Y. Yamaguchi, M. Kunitake, J. Electroanal. Chem. 566 (2004) 323.

[24] W. Zheng, M. M. Maye, F. L. Leibowitz, C. J. Zhong, Anal. Chem. 72 (2000) 2190.

[25] E. L. Smith, C. A. Alves, J. W. Anderegg, M. D. Porter, L. M. Siperko, Langmuir 8 (1992) 2707; D. E. Weisshaar, M. M. Walczak, M. D. Porter, Langmuir 9 (1993) 323; D. R. Jung, A. W. Czanderna, Critical Rev. Solid State Mat. Sci. 19 (1994) 1.

Figure captions

Fig. 1. Schematic illustration of a carboxylic acid terminated self-assembled monolayer adsorbed onto atomically flat and nano-ordered topographical gold surfaces.

Fig. 2. Preparation of nano-ordered topographical gold surfaces.

Fig. 3. Tapping-mode AFM 3D images (a) for a gold-NPs modified Au/mica surface followed by heat-treatment, and the distribution of the height of its topographical surface (c). The cross-sectional view corresponds to the line drawn (b).

Fig. 4. Cyclic voltammograms for the reductive desorption of a CDT-modified NPs-Au/mica electrode (geometric area: 0.264 cm^{-2}) (a) and a Au/mica electrode (geometric area: 0.268 cm^{-2}) (b) in 0.1 mol dm^{-3} KOH solution. Potential sweep rate: 50 mVs^{-1}.

Fig. 5 Schematic illustrations for surface topographical model.

Fig. 6 Schematic illustrations for adsorbed molecular models of CDT on atomically flat (A) and nano-ordered topographical (inter-hemispherical nanoparticle distance: 0 (B), 1 (C) and 2 (D) nm) surfaces.

Fig. 7. Cyclic voltammograms of 1 mmol dm^{-3} $[Ru(NH_3)_6]^{3+}$ at a CDT-modified NPs-Au/mica electrode at various pH values (5 mmol dm^{-3} HCl + 5 mmol dm^{-3} NaOH). Potential sweep rate: 20 mVs^{-1}. Geometric electrode area: 0.246 cm^2.

Fig. 8. Change in the anodic peak current of 1 mmol dm^{-3} $[Ru(NH_3)_6]^{3+}$ at CDT-modified NPs-Au/mica (a) and Au/mica (b) electrodes at various pH values, and simulated fitting curves using pKa = 6.0 . Potential sweep rate: 20 mVs^{-1}. Geometric electrode area: 0.246 cm^2.

Fig. 9. pH dependence of the FTIR spectra for CDT-modified NPs-Au/mica and Au/mica surfaces.

Fig. 10. Change in the peak area ratio for the symmetric $–COO^-$ stretching band against that for the C=O stretching band of –COOH, as a function of pH for CDT-modified NPs-Au/mica and Au/mica surfaces.

Figure1

Click here to download high resolution image

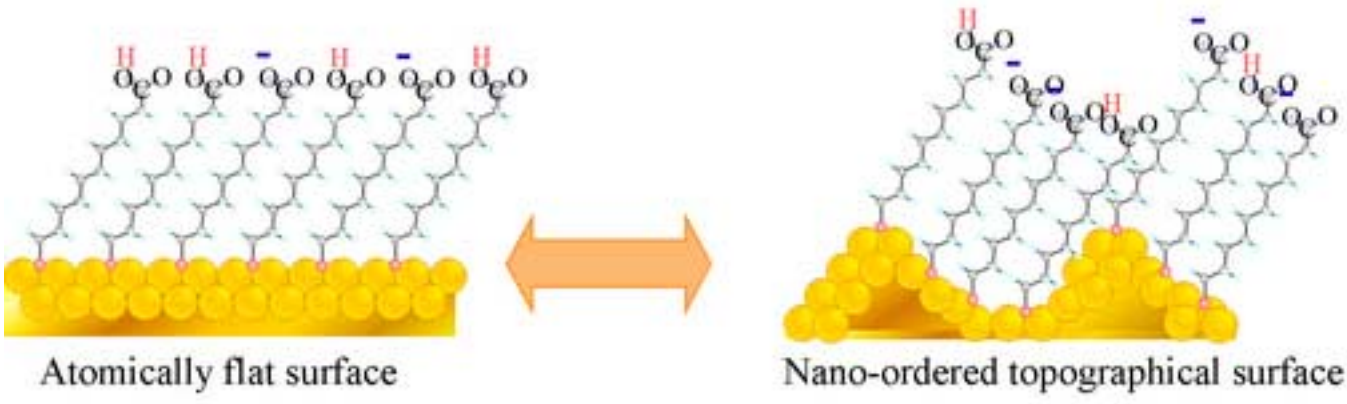

Fig. 1

Figure2

Click here to download high resolution image

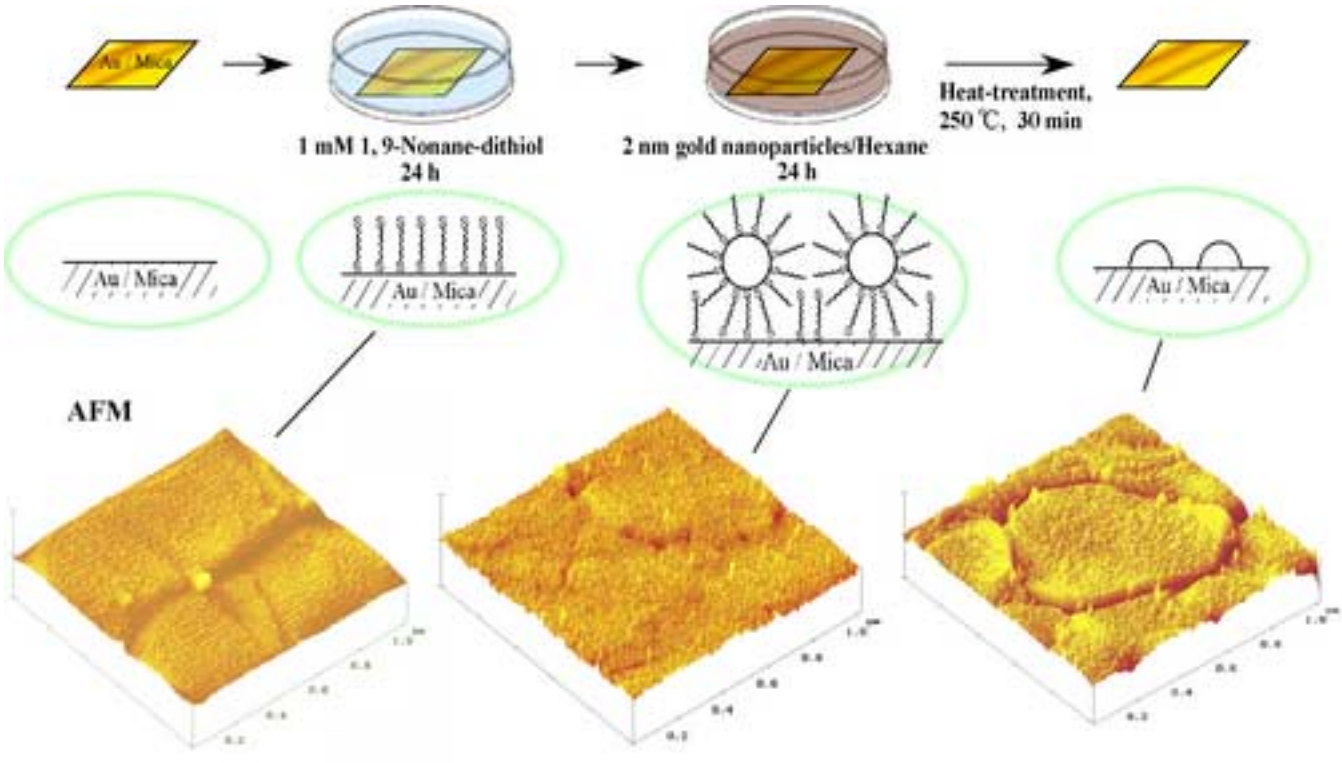

Fig. 2

Figure3
Click here to download high resolution image

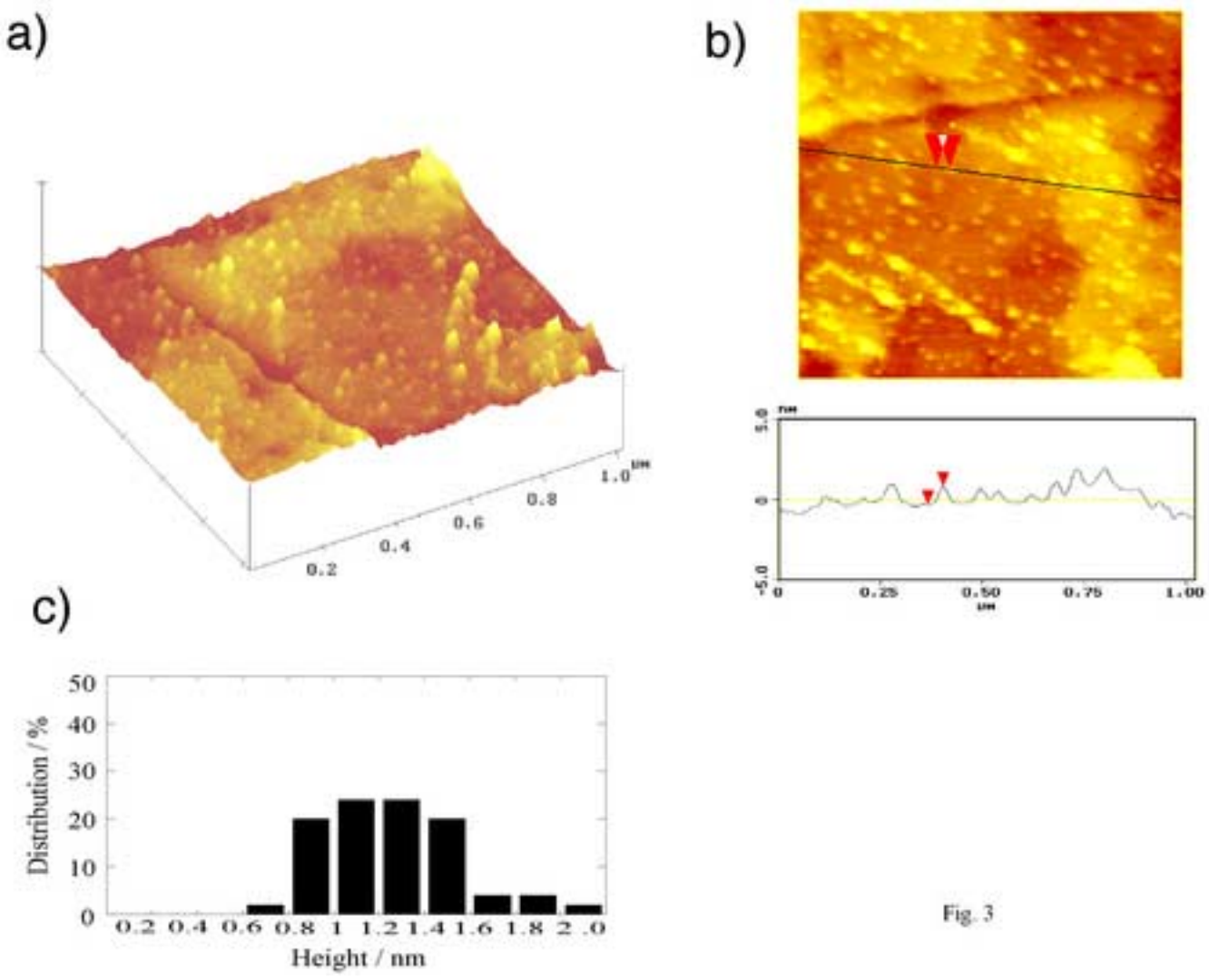

Fig. 3

Figure4
Click here to download high resolution image

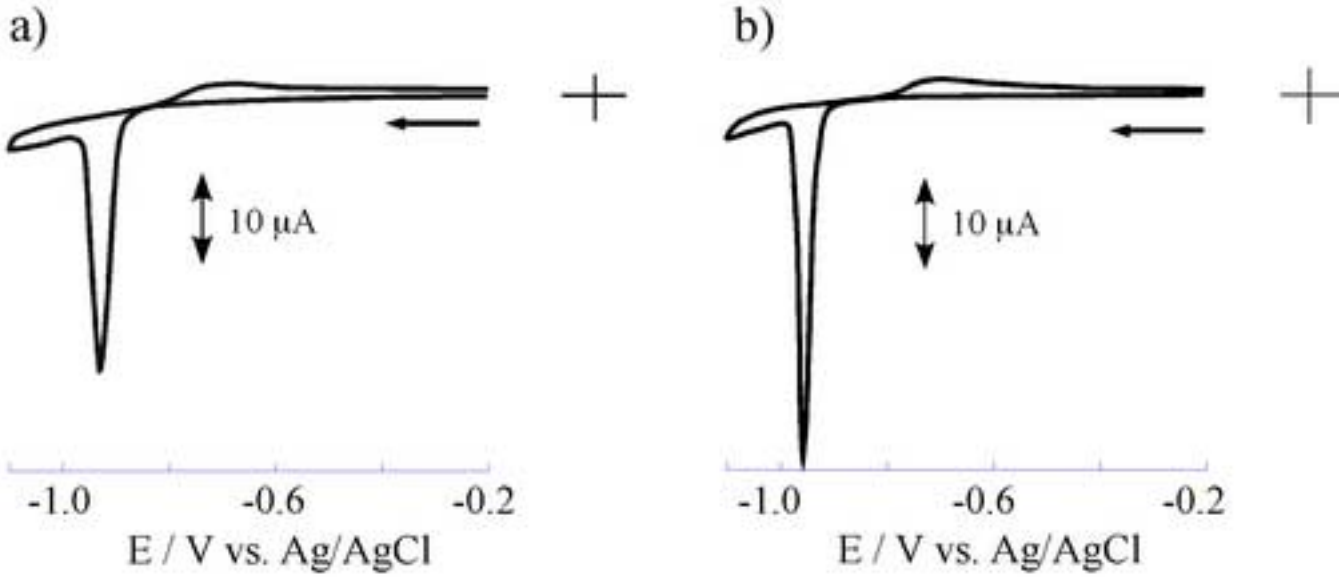

Fig. 4

Figure5
Click here to download high resolution image

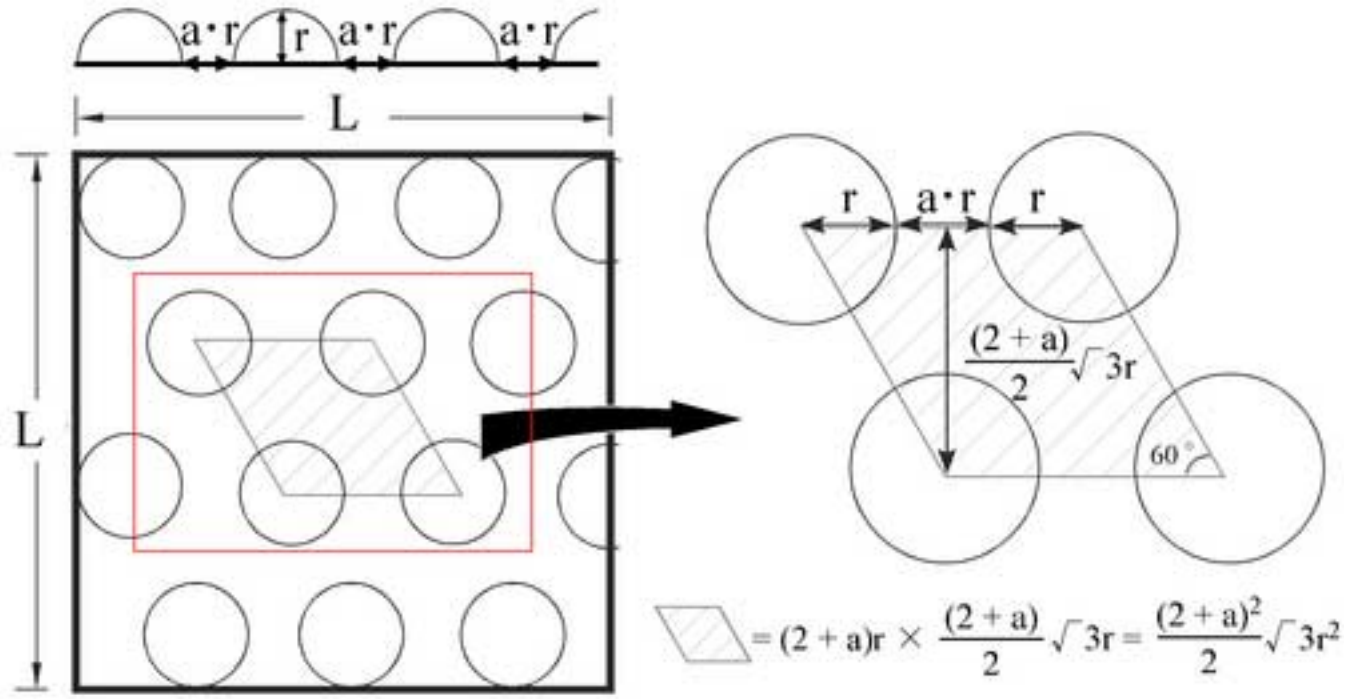

Fig. 5

Figure6

Click here to download high resolution image

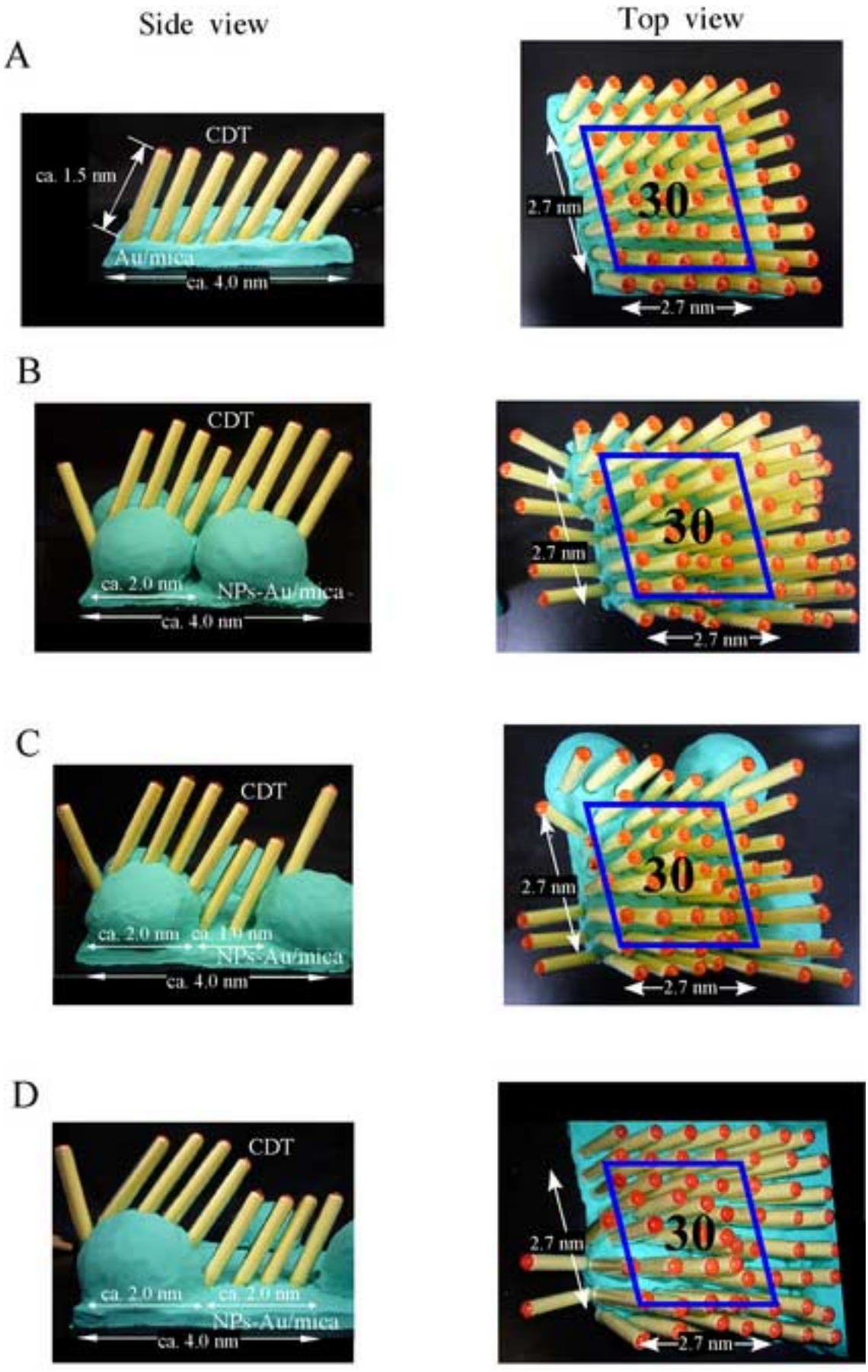

Fig. 6

Figure7
Click here to download high resolution image

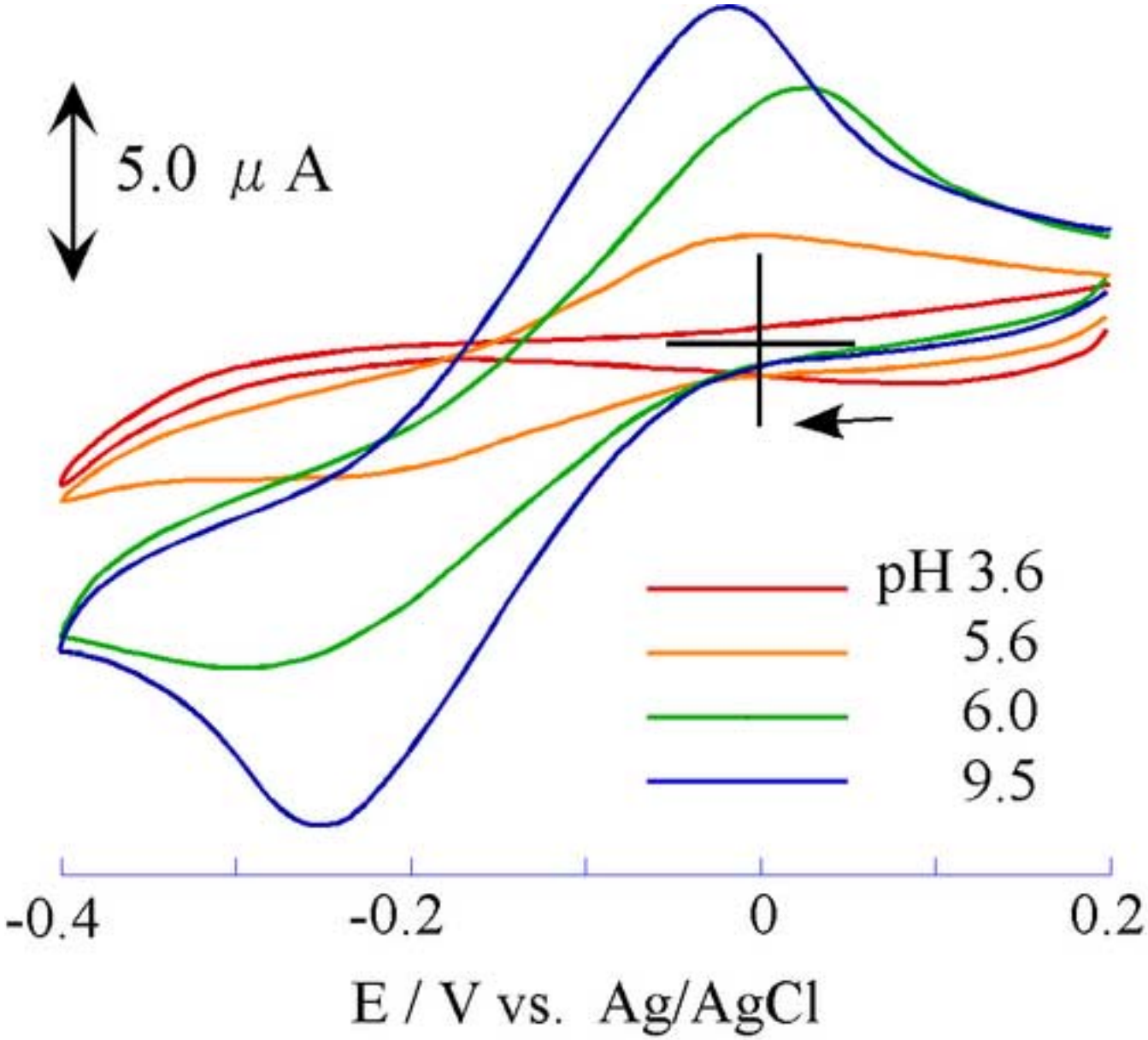

Fig. 7

Figure8
Click here to download high resolution image

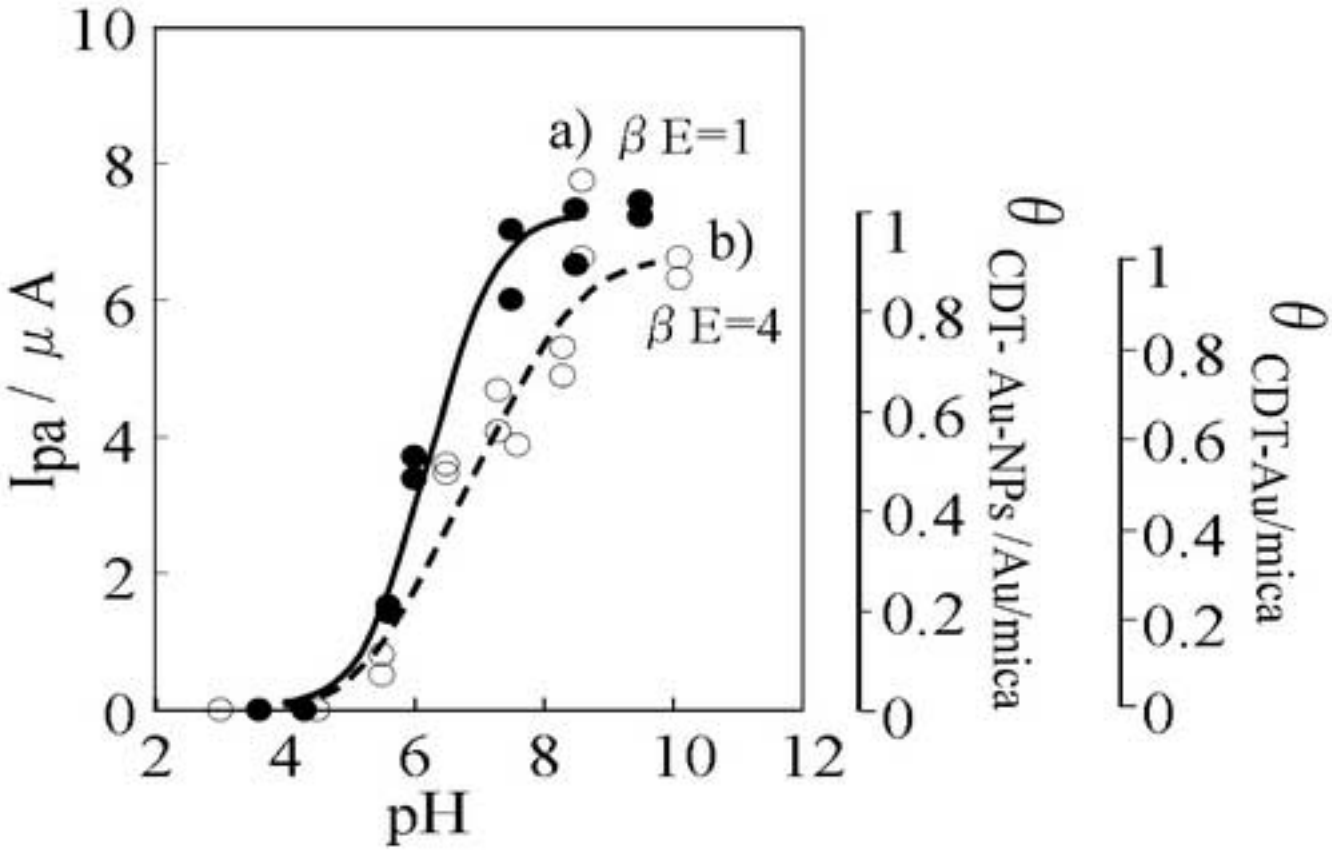

Fig. 8

Figure9
Click here to download high resolution image

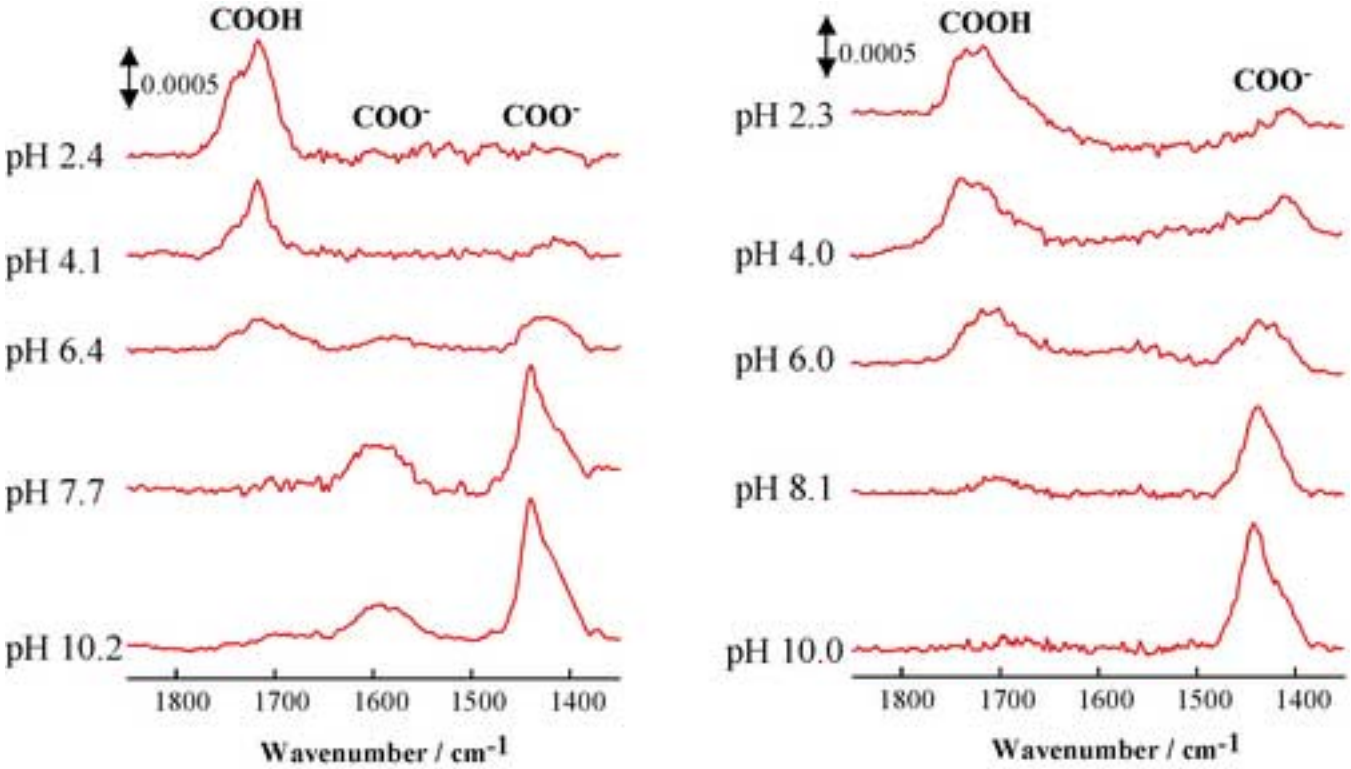

Fig. 9

Figure10
Click here to download high resolution image

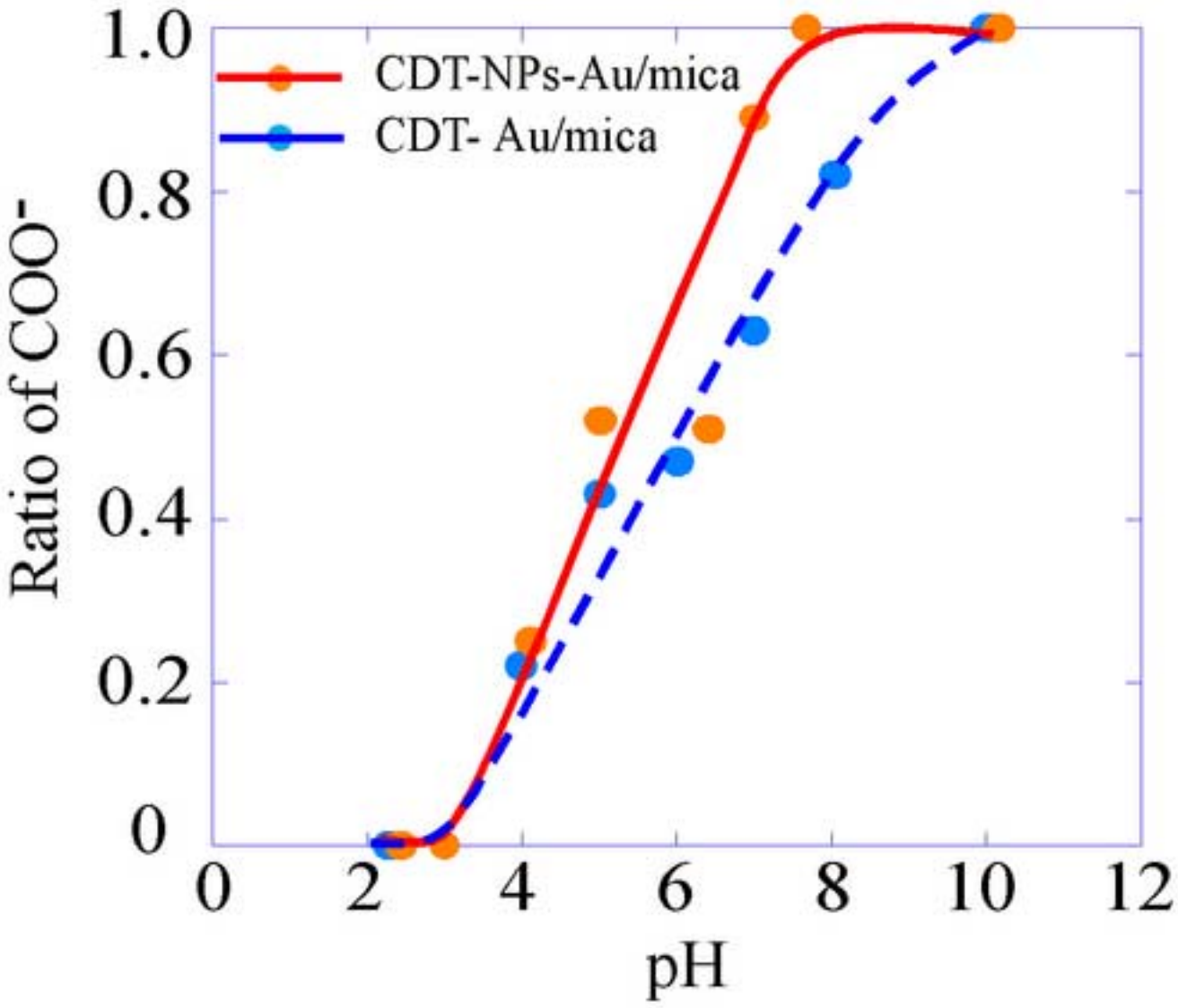

Fig. 10